Kinetics of Association of Anti-lysozyme Monoclonal Antibody D44.1 and Hen-Egg Lysozyme

Gioia Altobelli* and Shankar Subramaniam*†‡

*National Center for Supercomputing Applications, †Center for Biophysics and Computational Biology, Departments of Biochemistry, Molecular & Integrative Physiology and Chemical Engineering and Beckman Institute for Advanced Science and Technology, University of Illinois at Urbana-Champaign, Urbana Illinois, 61801, and ‡Departments of Bioengineering and Chemistry and Biochemistry, University of California at San Diego, La Jolla, California 92093 USA

ABSTRACT Association rate constants for antigen/antibody associations have been computed by Brownian Dynamics simulations of D. L. Ermak and J. A. McCammon, *J. Chem. Phys.* 69:1352–1360, 1978. The model of monoclonal antibody (mAb) D44.1 is based on crystallographic data (B. C. Braden et al., *J. Mol. Biol.* 243:767–781, 1994). Electrostatic forces that steer the antigen to the antibody-combining site are computed by solving the linearized Poisson–Boltzmann equation. D44.1-HEL complex displays very similar association motifs to a related anti-lysozyme antibody, HyHEL-5-HEL system. The computed association rate constants are comparable in the two systems, although the experimental affinity constants differ by three orders of magnitude (D. Tello et al., *Biochem. Soc. Trans.* 21:943–946, 1993; K. A. Hibbits et al., *Biochemistry.* 33:3584–3590, 1994). Simulations suggest that the origin of the differences in the affinity come from dissociation rate constants. We have also carried out simulation experiments on a number of mutant antibody fragment–HEL associations to address the role of electrostatics and, to a limited extent, the orientational aspects of association.

INTRODUCTION

The kinetics of association in the humoral immune system has been extensively studied, after the development of the hybridoma technology (Kohler and Milstein, 1975; Winter and Milstein, 1991). The association of antibody fragments with protein antigens is thought to be characterized by second-order rate constants in the range of 10^{6-1} (Raman et al. 1992; Foote and Eisen, 1995; Hibbits et al., 1994; Northrup and Erickson, 1992). The viscosity dependence of these rate constants shows that the association is diffusion-limited (Raman et al., 1992; Xavier and Willson, 1998; J. Foote, personal communication). In the diffusion-controlled regime of reactions in solution, the rate constant is governed by the rate at which the reactant particles diffuse through the medium. The steady-state rate of diffusion-controlled reactions was first established by the classic work of Smoluchowski (1917). It is proportional to the relative diffusion constant D (Einstein's coefficient), which is approximately the sum of the individual diffusion constants for the two species (neutral and of spherical shape) that will undergo the reaction (Hynes, 1985).

The long-range forces generated by the charge distributions on the reactants can enhance the reaction rate of association by steering them toward each other. Several other factors may also be important, such as relative orientation of the combining sites, short-range solvent structural forces, hydrodynamic interactions, and flexibility of the reacting molecules upon binding (induced-fit or gating). For systems with complex geometry, such as in the case of an antibody association with an antigen, analytical solutions are not feasible. A numerical simulation method, where some of the features of the system are coarse-grained, serves as the best approach for computing reaction rates (Hynes, 1985). In particular, the Brownian Dynamics (BD) method allows one to simulate the long-time behavior of model systems, and to evaluate rate constants of diffusion-limited associations (Ermak and McCammon, 1978). From a large number of Brownian trajectories, a description of an ensemble of diffusing particles is generated, provided that the simulation time step chosen is much greater than the solvent collision time (Van Kampen, 1992; Chandrasekhar, 1946).

Our computer simulations of the bimolecular rate constants for a monoclonal antibody fragment and its antigen have been carried out within the framework of the BD theory, using the method described in Northrup et al. (1984). This method has been already successfully applied to several other systems, including the association of a monoclonal antibody, HyHEL-5, with the antigen hen egg lysozyme, HEL (Kozack and Subramaniam, 1993; Kozack et al., 1995). Electrostatic interactions (long-range forces) between the two reactants are included in our model as a basic feature, along with exclusion forces. No hydrodynamic and short range forces are modeled, and no flexibility is allowed for both of the proteins in our simulations. The specific diffusional association we consider here is the complexation of the D44.1 monoclonal antibody fragment Fv and its protein antigen HEL.

The two associations, D44.1-HEL and HyHEL-5, differ in affinity, but the two monoclonal antibody fragments share common binding motifs both on the antibody and on

Received for publication 21 April 1999 and in final form 9 August 2000.

Address reprint requests to Shankar Subramaniam, Departments of Bioengineering and Chemistry and Biochemistry, University of California at San Diego, La Jolla, CA 92037.

Dr. Altobelli is an Istituto Pasteur–Fondazione Cenci Bolognetti Fellow. His present address is Karolinska Institute, Center for Structural Biochemistry, Novum, S-141 57 Huddinge, Sweden.

0006-3495/00/12/2954/12 $2.00

the lysozyme. Crystallographic data (Braden et al., 1994) show that D44.1 binds to a HEL epitope at the center of which is two arginine residues, Y 45 and Y-68 (Y denotes HEL, whereas H and L denote the heavy and light chains of the antibody, respectively). Two glutamate residues, H 35 and H 50, of the antibody fragment are key features of the antibody's combining site (Fig. 1). Both epitope and paratope of the D44.1-HEL complex are very similar to those of HyHEL-5-HEL. In both associations, three salt bridges are formed between the two glutamates and the two arginines, in such a way that H 35 is linked to Y 68, and H 50 to both Y 45 and Y 68. Major differences between the two associations are observed in terms of number of water molecules involved at the interface (one of the salt links, the one between H 50 and Y 68, is mediated by a water molecule in the HyHEL-5-HEL complex), dipolar interactions (only a couple of them are similar in the two complexes), and local geometry (the side chain of Y 45 is slightly tilted in the D44.1-HEL complex). Calorimetric studies showed that both reactions are enthalpically driven with an unfavorable entropic contribution (Schwartz et al., 1995; Hibbits et al., 1994). A systematic comparison of the interfacial regions of the two complexes was performed by Gibas et al., (1997), and a review of energetics and kinetics of a number of monoclonal antibodies complexations with the protein antigen HEL can be found in Braden and Poljack (1995) and Davies and Cohen (1996).

In the treatment of the diffusing molecule, the antigen, we used a simple description that takes advantage of the almost spherical shape of the lysozyme. HEL is modeled both as a sphere of radius 4 Å that bears a charge +2e, and as a combination of spheres of different size and charge. The probe charge, +2e, simply describes properties of a specific group of atoms, namely the two arginines Y 45 and Y 68 in the HEL epitope. To take into account the orientational constraints in our protein–protein association problem, we defined a reactive patch on the small sphere that represents the epitope region of HEL. The presence of such a reactive patch on the diffusing sphere has the effect to decrease the on-rate constant, rescaling the sphere-computed reaction probability by a factor that is related to the size of the patch. Size of the patch was estimated based on crystallographic data, and was meant to represent an averaged distribution of favorable orientations. Computation of interaction energies for many different relative orientations in Barnase–Barstar showed that the favorable orientation is the one observed in the crystallographic structure (Gabdoulline and Wade, 1997). More sophisticated atom-based models of reactants has recently been addressed by Gabdoulline and Wade (1999).

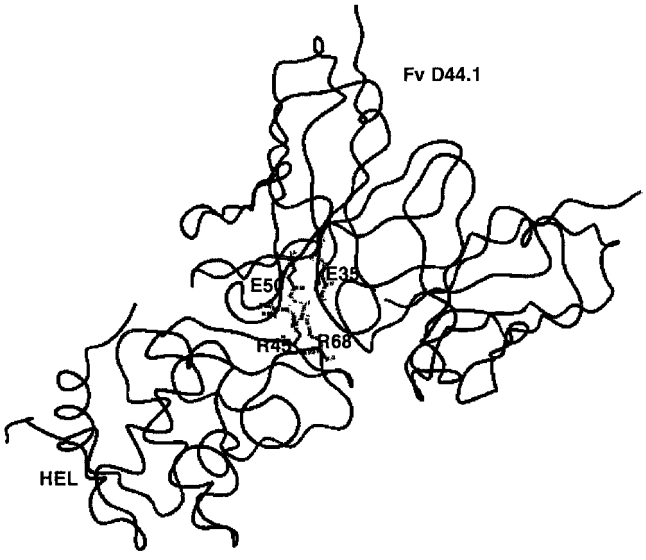

FIGURE 1 Carbon-alpha ribbon model of the complex FvD44.1-HEL, based on crystallographic data. Side chains of key residues in paratope (H: E35 and E50) and epitope (Y: R45 and R68) are also displayed. The four residues form three salt bridges (Braden et al., 1994). The Fv antibody fragment is made of the variable domains of the engineered fragment Fab (data extracted from Brookhaven Protein Data Bank, access code: 1mcl.)

The model of the Fv fragment of the antibody was built at the atomic level of detail; i.e., each atom held its own charge, radius, and crystallographic coordinates. Test charge approximation was used to compute the forces acting on the antigen: the force experienced by the diffusing particle is evaluated at each point of the diffusional space as the product of the lysozyme model's charge and the electrostatic potential generated by the target molecule (the antibody fragment Fv). The overall charge on the wild-type Fv fragment was −1e; the antibody's charge description corresponds to a model of its protonation state at pH = 7. Previous studies using test charge models on antibody–lysozyme system have yielded relative association rate constants comparable to those obtained experimentally from stopped-flow measurements (Kozack et al., 1995). Crystallographic studies of hen egg lysozyme in the complexed and uncomplexed state reveal only small conformational changes (Braden et al., 1994) and, hence, conformational flexibility of the reactants during association was not addressed in this work.

The goal of this study was to simulate the on-rate constants for the D44.1/HEL association, and calculate relative reaction rates for some selected mutant associations. We compared results obtained for the D44.1-HEL system to the ones available for the HyHEL-5-HEL association. To investigate the role of the electrostatic steering in the underlying molecular recognition process, we modeled point mutations in the antibody fragment, and assessed the resulting variation of the reaction rates at a physiological ionic strength. This will aid in understanding the role of single residues (point mutations) and possible interactions between pairs of them (double mutations) toward the association.

MATERIALS AND METHODS

Electrostatics and Brownian Dynamics

The electrostatic potential ϕ due to the charge distribution on residues of the antibody in electrolyte solution obeys the Poisson–Boltzmann equation,

$$-\nabla \cdot \varepsilon \nabla u + \varepsilon \kappa^2 \sinh u = \frac{e\rho}{kT}; \quad u = \frac{e\phi}{kT}, \tag{1}$$

where ρ is the charge density of the antibody containing all the crystallographic information; e is the elementary unit of charge; k is the Boltzmann constant; ε is the position-dependent permitivity that combines solvent and internal permitivities with solvent probe radius and atomic radii; T is the temperature; and κ is the inverse Debye length, which is proportional to the square root of the ionic strength, I. Note that the electrostatic potential ϕ is a potential of mean force. We used the linearized version of Eq. 1, the linear Poisson–Boltzmann equation, corresponding to the assumption $\sinh u \sim u$. The linear Poisson–Boltzmann equation can be numerically solved for arbitrary shape of the target protein surface by a discretized continuum method (Warwicker and Watson, 1982; Davis and McCammon, 1990). We set the dimensions of our potential grid to $65 \times 65 \times 65$ and grid spacing to 1.2 Å.

The Brownian displacement of the antigen with respect to the antibody, Δr, at a certain temperature T and in the diffusional limit, is computed by the algorithm of Ermak and McCammon (1978),

$$\Delta r = (kT)^{-1} DF\Delta t + S, \tag{2}$$

where Δt is the time step, D is the Einstein's diffusion constant, F is the (electrostatic) force vector, and S is a random force vector that represents the action of the solvent on the diffusing antigen. Its components should have the following properties ($\alpha, \beta = x, y, z$):

$$\langle S_\alpha \rangle = 0 \quad \langle S_\alpha S_\beta \rangle = 2D\delta_{\alpha\beta}\Delta t. \tag{3}$$

To perform our simulations, we used the University of Houston Brownian Dynamics (UHBD) suite of computer programs (Madura et al., 1995), which can solve the Poisson–Boltzmann equation for the antibody and compute trajectories in the configurational space of the reactive pair.

Trajectories start with the antigen at uniformly random positions at a center-to-center separation distance b, and terminate when either a reaction condition is satisfied or the intermolecular separation becomes greater than a cutoff distance q. The fraction of trajectories that satisfy a defined reaction criterion (see below) provides an estimation of reaction probability β for the reactive pair. The reaction probability β serves, in turn, to evaluate the rate constants according to the formula (Northrup et al., 1984; Madura et al., 1995),

$$k = k_D(b)\frac{\beta}{1 - (1 - \beta)k_D(b)/k_D(q)}, \tag{4}$$

where $k_D(x)$ is the analytical rate constant for the diffusion to a relative separation x (see Eq. A3 in the Appendix). Definition of the radius b is made in such a way that, when $x > b$, the intermolecular potential is symmetrical and can be treated analytically. In the simple case in which the diffusing particle does not experience any intermolecular force at separation distance $> b$, function $k(x)$ gives the Smoluchowski reaction rate for spherical molecules, $4\pi bD$. In our simulations, we set the b radius at the value of 80 **Å** and the cutoff distance q at 500 **Å**.

Orientation constraints

Reactive patch

The reaction probability β, computed using the single sphere model mentioned in the introduction, does not take into account any preferred orientation of the diffusing protein upon binding to the target protein. Yet, only a fraction of all possible orientations are reactive. Orientational constraints can be included as a factor corresponding to the fraction of reactive orientations, assuming the isotropy of the orientation space (Berg and von Hippel, 1985; Zhou, 1993). If a reactive patch of solid angle Ω' is defined on the diffusing sphere, the actual reaction probability β' would be

$$\beta_L \le \beta' \le \beta. \tag{5}$$

The lower bound, β_L, is given by

$$\beta_L = \beta * p, \tag{6}$$

where p, the probability that the antigen only reacts with its reactive patch properly oriented, is computed as

$$p \approx \frac{\Omega'}{4\pi}, \tag{7}$$

where 4π is the solid angle corresponding to the entire sphere surface. The solid angle Ω' of a spherical cap is

$$\Omega' = 2\pi \int_0^\theta d\theta' \sin(\theta') = 2\pi[1 - \cos(\theta)], \tag{8}$$

where 2π stands for the integral of the second angular coordinate ϕ. The scaling factor p, in terms of the angle θ, is then

$$p = \frac{1 - \cos(\theta)}{2} = \sin^2\left(\frac{\theta}{2}\right). \tag{9}$$

It can be shown (see the Appendix) that the rate constant of Eq. 4 should obey the restriction

$$k(\beta_L) \le k(\beta') \le k(\beta). \tag{10}$$

If the angle θ is small, as in our case, it is reasonable to expect that the actual probability, β', is $\beta' \approx \beta_L$. That is, when the patch is really small, it is likely that the antigen would not come back and react later after a first unsuccessful encounter. In this specific case, and only in this case, we can assume that the reaction rate constant in the presence of the patch will be close to the lower-bound value:

$$k(\beta_L) = k_D(b)\frac{\beta * p}{1 - (1 - \beta * p)k_D(b)/k_D(q)}. \tag{11}$$

Our estimate of the angle θ is based on the measure of the angle between the coordinates' vectors of the C_ζ atoms of the two arginines in the epitope, and it is half of this value, that is $\theta = 17.4°$. The corresponding scaling factor defined in Eq. 9 is 6×10^{-3}. The order of magnitude off the predicted absolute rates is expected to drop of about two orders, because it can be shown (see Appendix) that

$$k(\beta_L) \approx k(\beta) * p \tag{12}$$

Dependence of the scaling factor p on the angle of the reactive patch, θ, is such that when θ ranges within 8° and 22°, its order of magnitude is still 10^{-3}. As shown by Eq. 12, the magnitude of the reaction rate is essentially unaltered by variation of the reactive patch's angle in the range mentioned above.

Dumbbell model

An asymmetric dumbbell composed by two spheres of different sizes was also used to take into account the orientational constraints. The smaller

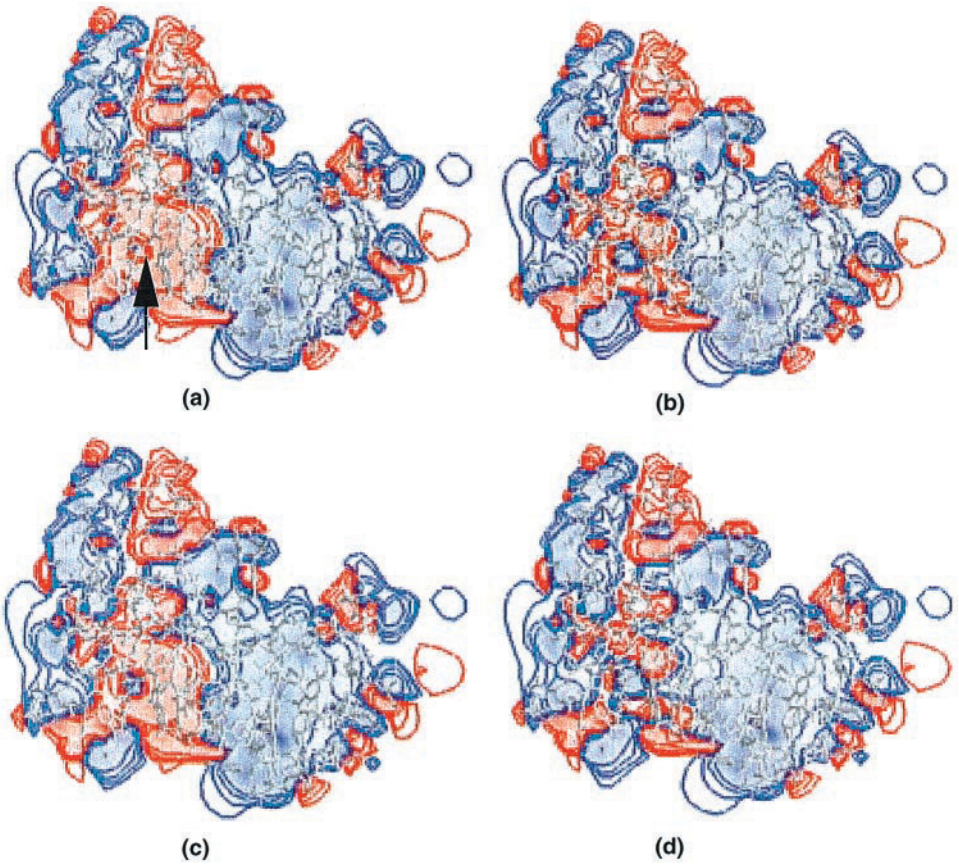

FIGURE 2 Electrostatic potentials: two-dimensional contour maps in (*a*) WT antibody fragment, (*b*) mutant E35Q, (*c*) mutant E50Q, and (*d*) DMU. Sections are obtained by slicing with a plane through the average of *z* coordinates of CD atoms of residues H 35 and H 50. An arrow in map (*a*) points to these two key residues. The same orientation was retained for the mutant fragments in maps (*b*), (*c*), and (*d*). Red contours correspond to potential values −0.5, −1, −2 and −4 KT; Blue contours represent potential values 0.5, 1, 2, and 4 KT. Overall charge of the WT fragment is −1e; the two single mutants E35Q and E50Q are neutral, whereas the DMU fragment has a net positive charge: +1e.

sphere of the dumbbell is analogous to the sphere model previously mentioned, and hence bears a charge of +2e and has radius of 4 **Å**; the larger one has a radius of 20 **Å** and a charge either +6e or zero. The dumbbell is kept rigid during the trajectory simulations, using a line of centers technique, and the distance between the two centers is 24 **Å**, i.e., the sum of the two radii (Kozack et al., 1995). Orientation constraints introduced by the dumbbell are less strict than the ones provided by the spherical patch. Electrostatic torque operating on the dumbbell was not taken into account. Reaction criteria used in the models, reactive patch and dumbbell, are described in the following section.

Model system details and simulation parameters

The 2.5-Å resolution x-ray coordinates of the monoclonal antibody/antigen complex were extracted from the Brookhaven Protein Data Bank (access code: 1mcl). The pdb file was modified to remove crystallographic water and add polar hydrogens. The latter step was necessary because the charge table for the antibody was parameterized for molecules with polar hydrogen atoms (CHARMM data set). A program, NACCESS (Hubbard and Thornton, 1993), was iteratively used for removing the crystallographic water molecules, and hydrogens were added using the HBUILD program within QUANTA molecular graphics package (QUANTA, 1996). Mutations were produced by merely substituting oxygen (nitrogen) atom with nitrogen (oxygen) one in the side chain of glutamic acids (glutamines) and aspartic acids (asparagines). No optimization of mutant side chains was carried out. We also mutated the key glutamate residues to arginines as a test on steering. In that case, side-chain modeling was performed.

Because the crystallographic data mentioned above describe the antibody fragment Fab, we further modified the pdb file to obtain the Fv structure. Fab is a monovalent antigen-binding fragment consisting of variable and constant domains of the heavy chain, V_H and C_{H1}, plus variable and constant domains of the light chain V_L and C_L, whereas Fv is made of the variable domains only (Winter and Milstein, 1991). Immunoglobulins IgG produced via hybridoma technique and their fragments, Fab and Fv, yield comparable binding affinities (Bhat et al., 1990; Schwartz et al., 1995). A "hydrogenized" Fv fragment of the D44.1 contains 2154 atoms, and is made of 224 residues, 108 of them belonging to the light chain. Indeed, 41 of the putative titrating sites were defined as net point charge sites in our fragment. They were assigned to specific atoms of glutamate, aspartate, lysine, arginine side chains, and to N/C termini. The overall (net) charge resulting from the summation of positive and negative charges of those sites was −1e in the wild-type fragment. Mutations of aspartates and glutamates were done by substitution of the carboxyl group by the amide group. A few of the glutamines and asparagines that are in proximity of the binding region were also selected for mutations into glutamate and aspartate residues, respectively.

The interface region of the complex is seen in the x-ray structure to be flat, and no important structural changes are assumed upon HEL binding (Braden et al., 1994). We also assumed that both the key residues, H 35 and H 50, were adequately solvent exposed and on the surface where they could make contacts with lysozyme. Thus, two contact association criteria were adopted in which both of the key residues were taken into account. The reaction condition for a first set of sphere-model simulations is such that the center of the diffusing particle should come within 9.0 Å of atom C_δ of H 50 of the target. At that distance, the model antigen HEL, a sphere of radius 4.0 Å, is in van der Waals contact with the combining site residues on D44.1 (one distance criterion, C1). A second set of simulations was carried out with a different definition of the binding site of the

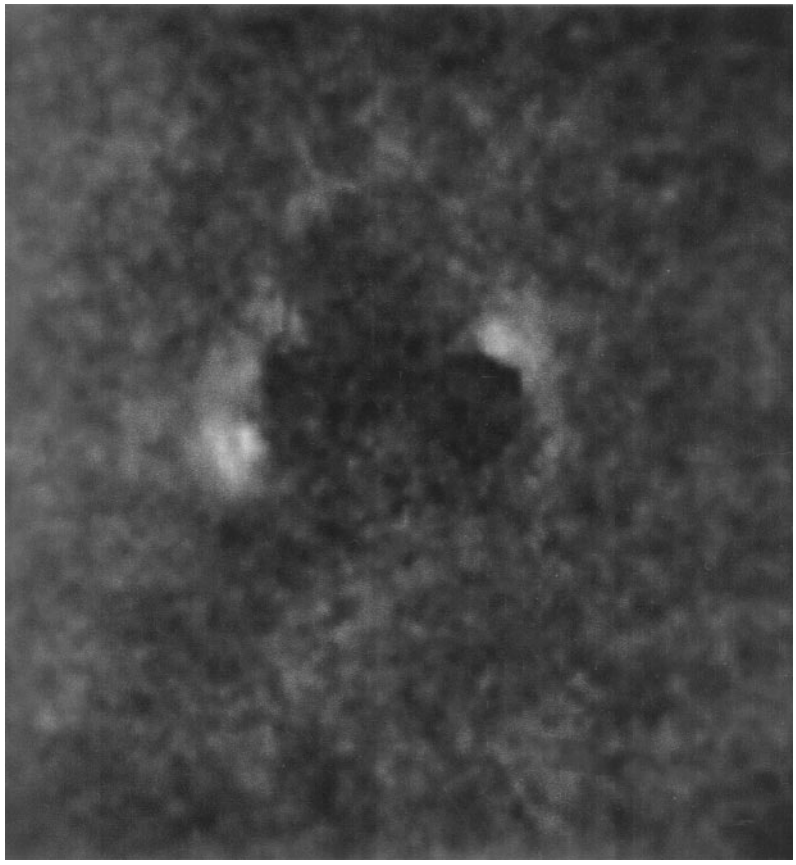

FIGURE 3 Volume rendering of the antigen's position sampled at 50-ps intervals from 10,000 trajectories from wild-type complexation. The brightest area displays the binding site (atom C_δ of H 50), confirming that the antigen is steered by the key residues H 35 and H 50. A decoy site is in a location that would not be exposed to the solvent in the fragment Fab and in the parent immunoglobulin IgG.

antibody, introducing a second reaction condition in addition to previous one. The second reaction condition is such that the center of the HEL model should be at 12 Å from the C_δ of the H 35 (two-distance criterion, C2). The reaction criterion for the dumbbell was defined in terms of distance of the center of the small sphere from the C_δ atom of H 35. Reaction distance was set to 7.5 Å, which provided relative errors of 7–8% on the reaction probability, depending on the overall charge of the dumbbell.

A variable time steps combination was used to save computational time with no loss of accuracy, in which the basic time step was 1 ps. Temperature was set to 300 K and pH to 7. Dielectric constants were assigned value 2 in the interior of the target protein and 78 in the solvent region. Forces introduced in the Brownian Dynamics algorithm were computed in the test charge approximation with a lysozyme charge +2e. A diffusion coefficient, corresponding to a hydrodynamic radii of 30 Å to the antibody and 4 Å to antigen, was set to 0.0695 $Å^2$/ps. In the simulations with dumbbell, the relative diffusion coefficient was 0.022 $Å^2$/ps, which is the value estimated by the UHBD program during the simulation, and which is close to the experimental value 0.0152 $Å^2$/ps reported in literature (see, for example, Xavier and Willson, 1998.) Viscosity of the solvent at $T = 300$ K is 0.89 cp, a value that is close to that of a saline solution (viscosity of water is 0.1 cp). Ionic strength's dependence of the rate constant was explored in the range of low to physiological values. Each absolute reaction rate constant for wild type and mutants was obtained by running 60,000 trajectories with single sphere model, on a Silicon Graphics Power Challenge array of supercomputers. Simulation of 20,000 trajectories required 4–12 h of CPU time, depending on the specific association. Dumbbell simulations required 100,000 trajectories, and computational time was about 20 times longer than the corresponding time in simulations with sphere model.

RESULTS

Electrostatic steering

In Fig. 2, two-dimensional contour electrostatic potential maps are shown, for the wild-type fragment (*a*) and for three of its mutant fragments. Mutants were obtained by neutralization of the negative charge of the antibody binding site's residues H 35 and H 50: single mutant E35Q (*b*), single mutant E50Q (*c*), and double mutant (DMU) combination of both mutations E35Q and E50Q (*d*). Potential maps were produced, slicing with *z*-plane through the average *z*-coordinate of atom C_δ of residues H 35 and H 50. "Key" residues H 35 and H 50 are pointed by an arrow in (*a*) to help to focus on the binding region of the antibody fragment. The same orientation was kept for the antibody fragments in all maps of Fig. 2. The red color shows negative contours corresponding to -0.5, -1, -2, and -4 kT; blue shows positive contours 0.5, 1, 2, and 4 kT. In (*a*), the binding region of the wild-type fragment is uniformly negative, whereas, in (*b*), (*c*), and (*d*), this uniformity is broken, and positive regions appear. Maps displayed in Fig. 2 were built from UHBD potential grids imported into the graphics package GRASP (1991). A volume rendering of antigen-position density is shown in Fig. 3 for a simulation of 10,000 trajectories with wild-type fragment. The position of

the antigen was recorded every 50 ps during the simulation. Antigen is steered toward the binding site, as shown by the brightest spot in the cloud. The picture was obtained displaying data with Renderman visualization package (resolution is 2 Å). A second area of high density corresponds to a "decoy site" on the antibody fragment.

Ionic strength dependence of key mutant associations

In Fig. 4, relative rates for single mutations E35Q and E50Q, and DMU, are compared. Simulations were performed with the single reaction criterion C1, and error bars were evaluated according to an error propagation formula. Statistical errors are obtained over 60,000 trajectories for all the associations studied (see also the caption of Fig. 4). Each of the two single mutations, E35Q or E50Q, render the Fv fragment globally neutral. The DMU results in a net positive charge (+1e) of the antibody fragment. Data collected using both criteria, C1 and C2, are represented in Fig. 5. E35Q relative association rates are compared in Fig. 5 *A*. Predicted changes of relative rates with ionic strength are consistent. Differences, however, appear in the case of E50Q and DMU (Fig. 5, *B* and *C*, respectively). Data relevant to the associations are collected in Table 1. Comparison of WT type absolute rates with C1 and C2 shows that the two criteria produce fairly different values: At I = 150 mM, the rate computed using C2 is 24% less than the rate computed using C1 (see Table 2). Similar quantitative differences appear in the relative rates of E50Q and DMU mutants, whereas associations involving mutant fragment

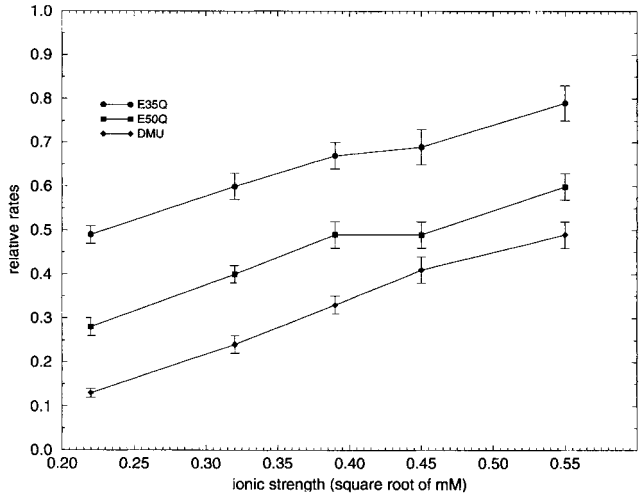

FIGURE 4 Ionic strength variation of relative reaction rates for two single mutants involving the key residues H 35 and H 50 (E35Q and E50Q, respectively), and a DMU that is the combination of the previous two mutations. Error bars on relative rates are evaluated with error propagation formulae. Statistical errors for each set of simulations is SEM × (1 − mean)/60,000, because the total number of trajectories is 60,000.

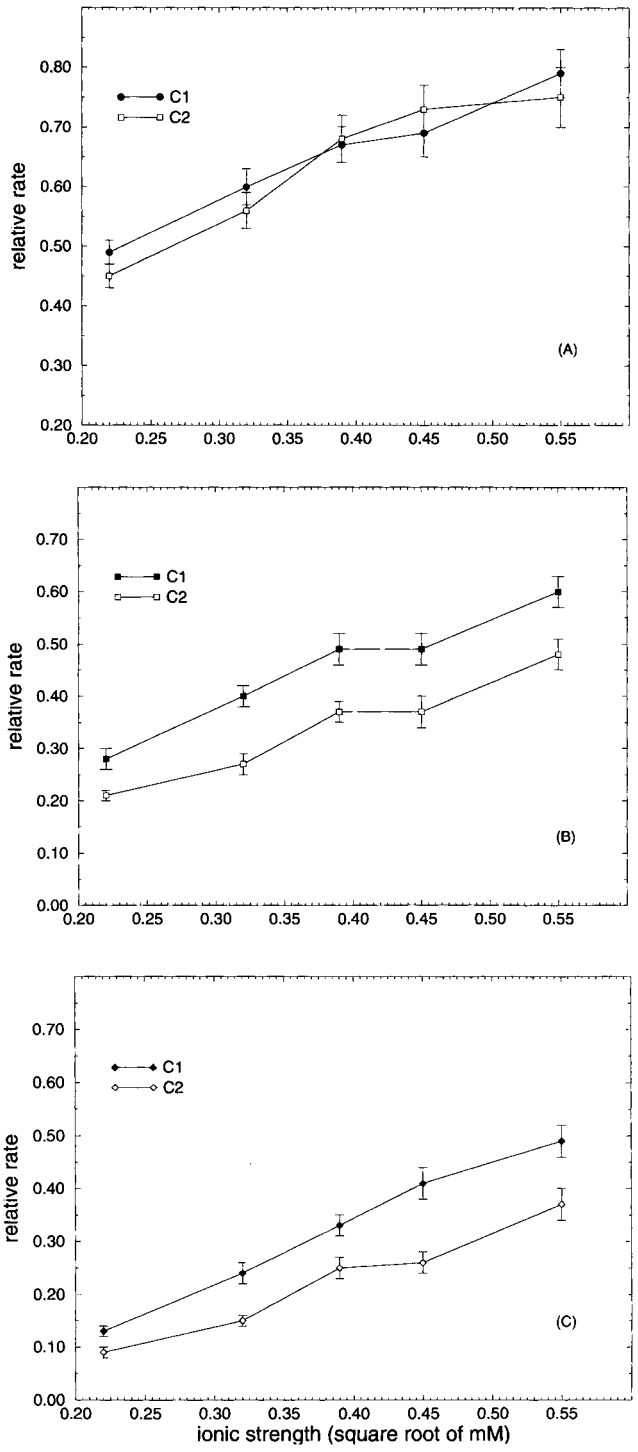

FIGURE 5 Comparison between ionic strength dependence of relative rates computed using one-distance criterion (C1) and two-distance criterion (C2), for a single mutant involving (*A*) residue H 35, E35Q, (*B*) residue H 50, E50Q, and (*C*) for a DMU involving both the two key residues of the binding site, E35Q + E50Q. Error bars as in caption of Fig. 4. Differences between relative rates computed with C1 and C2 that appear in the mutants arise from reduced electrostatic steering.

TABLE 1 Relative rate constants for key mutant associations*

Ionic Strength (mM)	E35Q	E50Q	DMU#
REACTION CRITERION C1			
50	0.49 ± 0.02	0.28 ± 0.02	0.13 ± 0.01
100	0.60 ± 0.03	0.40 ± 0.02	0.23 ± 0.02
150	0.67 ± 0.03	0.49 ± 0.03	0.33 ± 0.02
200	0.69 ± 0.04	0.49 ± 0.03	0.41 ± 0.03
300	0.79 ± 0.04	0.60 ± 0.03	0.49 ± 0.03
REACTION CRITERION C2			
50	0.45 ± 0.02	0.21 ± 0.01	0.09 ± 0.01
100	0.56 ± 0.02	0.27 ± 0.02	0.15 ± 0.01
150	0.68 ± 0.04	0.37 ± 0.02	0.25 ± 0.02
200	0.73 ± 0.04	0.37 ± 0.03	0.26 ± 0.02
300	0.75 ± 0.05	0.48 ± 0.03	0.37 ± 0.03

*Relative rates are computed as k mutant/k wild type.
#Double mutation E35Q + E50Q.

TABLE 2 Absolute rate constant for wild-type associations

Ionic Strength (mM)	Fully Charged (+8e) (k·10^7 Ms^{-1})	Partially Charged (+2e) (k·10^7 Ms^{-1})
	DUMBBELL	
150	3.35±0.23	2.6±0.20
	SPHERICAL PATCH	
	C1* (k·10^6 Ms^{-1})	C2* (k·10^6 Ms^{-1})
50	6.73 ± 0.18	5.97 ± 0.17
100	5.41 ± 0.16	4.55 ± 0.15
150	4.69 ± 0.15	3.68 ± 0.13
200	4.27 ± 0.14	3.38 ± 0.13
300	3.82 ± 0.14	2.92 ± 0.12

*C1: one-distance association criterion; C2: two-distance association criterion.

E35Q seems not to be substantially affected by the reaction criterion. The differences can be due to the reduced electrostatic steering as in the case of the double mutant and of E50Q (see Discussion). Reaction rates for association involving mutations of both the key residues increase gradually as the ionic strength increases. The same behavior was observed for the association of HEL with the double mutant fragment. Mutations of the key glutamate residues (H 35 and H 50) into oppositely charged arginine residues yielded the expected results (not presented in the Tables) for association rate constants. H 50 mutation reduced the rate constants significantly more than H 35 mutation. We note that H 50 makes two salt-link contacts as opposed to H 35, which makes a single contact.

Absolute rate constant: spherical patch and dumbbell

In Fig. 6, a variation of the absolute rate with the ionic strength for WT association is displayed. Reaction rates were obtained by scaling the computed reaction probability with the probability factor defined in Eq. 9, which accounts for the orientation constraints. Decrease of the rate with increasing ionic strength seems to match the linear Debye–Hueckel's behavior of reaction in solution of a pair of ions that bear charges of opposite sign (salt kinetic effect). However, deviations are appreciable, as expected from the fact that, in our computational model, the antibody produces a non-centrosymmetric electrostatics field. Data are presented in Table 2. The lowest value is the one computed at ionic strength 300 mM. It corresponds to the limiting case in which long-range electrostatic forces are switched off, due to the screening of the high concentration of ions in the solution. At ionic strength 150 mM, 100,000 trajectories were also run, modeling the antigen both as a fully charged (+8e) and a partially charged (+2e) dumbbell. Reaction distance was set to 7.5 Å, which provided the best statistics for simulations with dumbbell. Relevant reaction-rate constants are shown in Table 2. Reaction rates computed with fully and partially charged dumbbell are comparable.

Selected single and double mutant associations

Figure 7 shows a three-dimensional view of a cluster of residues involved in the mutant antibody fragment studies. In Table 3, relative rates for single mutant associations are presented. The C1 criterion of reaction was used for all these simulations, in which ionic strength was set to $I = 150$ mM. Mutations are listed by distance of a specific atom (C_δ or C_ζ) of the mutated residues' side chain from the C_δ atoms

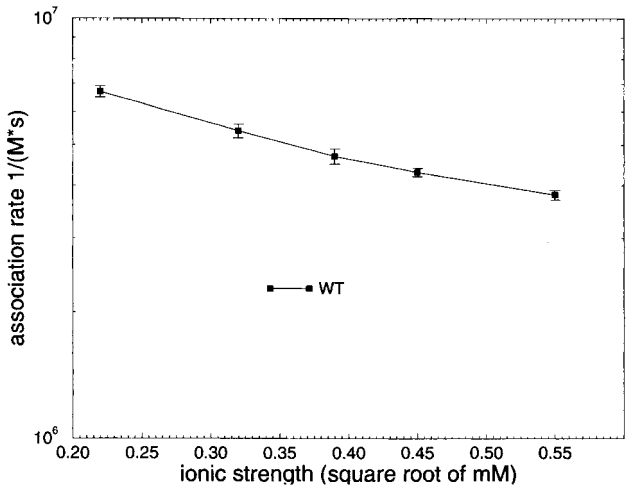

FIGURE 6 Absolute rate constant versus ionic strength in the wild-type association, computed with a spherical patch model. The lowest value of the rate, at ionic strength 300 mM, corresponds to the limiting case of no long-range forces, due to the screening of the ions in solution. Net charge on the antibody fragment is −1e.

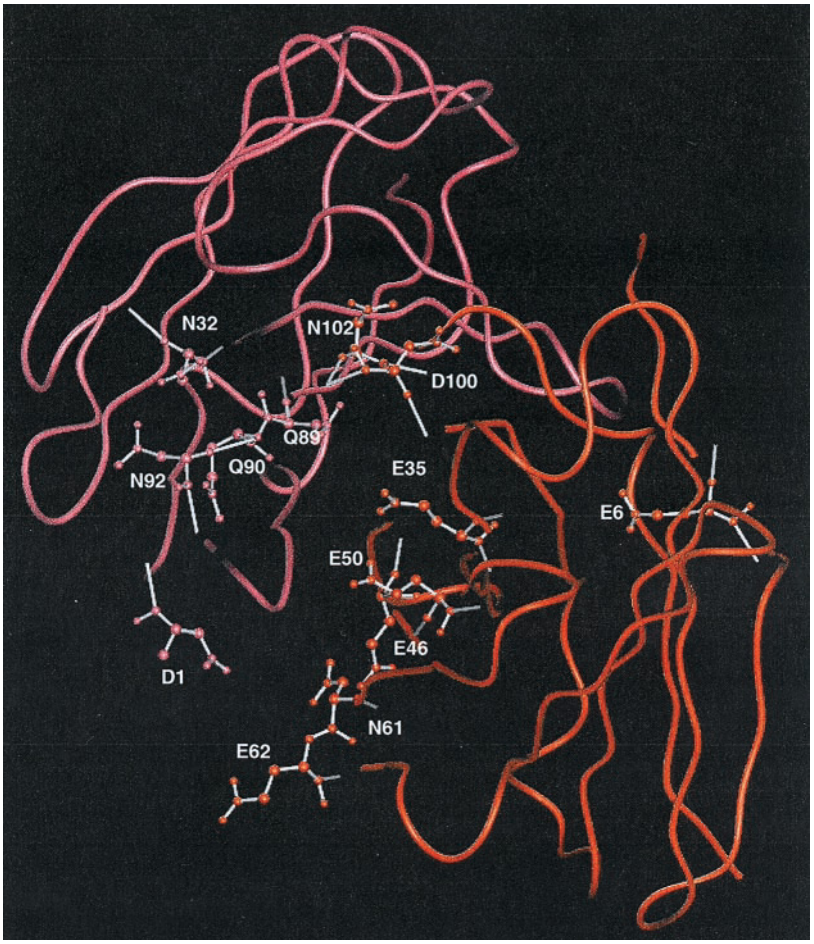

FIGURE 7 Residues involved simulation experiments of directed mutants, represented with ball-and-stick model. These residues are within a sphere of radius 20 Å from the binding site (atom C_δ of H 50). Domains V_L and V_H of the Fv fragment are shown in different colors (main chain only): light chain, L, in pink and heavy chain, H, in orange.

of H 35 and H 50. Mutations that produce a negative overall charge always increase the association rates (relative rates $>$ 1), while the mutations that produce a neutral or positive increment of charge result mostly in a decrease of the rate constant (relative rates $<$ 1).

TABLE 3 Relative association rate constants for single mutant associations

Type of Mutation*	Fragment Net Charge (e)	Distance From C·H 50\C·H 35 (Å)	Relative Rates (k mutant/k wt)
H: E50Q	0	0\4.98	0.49 ± 0.03
H: E35Q	0	4.98\0	0.67 ± 0.03
H: N61D	−2	10.37\11.44	1.08 ± 0.05
L: Q89E	−2	11.63\7.58	1.11 ± 0.05
L: Q90E	−2	12.15\10.65	1.17 ± 0.05
H: D100N	0	12.58\8.66	0.91 ± 0.04
L: D1N	0	13.72\14.39	1.00 ± 0.05
L: N92D	−2	14.15\13.42	1.27 ± 0.05
H: N102D	−2	14.47\10.06	1.16 ± 0.05
L: N32D	−2	14.65\12.71	1.26 ± 0.05
H: E62Q	0	15.11\17.83	0.91 ± 0.04
H: E46Q	0	15.34\14.57	1.09 ± 0.05
H: E6Q	0	16.44\13.64	0.98 ± 0.04

*Ionic strength = 150 mM. Mutated residues are within 20 Å from key residues (either H 50 or H 35) atoms C. H = heavy chain, L = light chain.

Mutation of residues proximal to H 35 and H 50 were not always the most effective, as seen in Table 3. The highest relative rates are due to the mutation of an asparagine in the light chain (L92:N92D), which is also the farthest asparagine. Examining the mutations that produce fragment net charge −2e, we found that reaction rates tend to cluster in two groups (within the statistical errors). Mutations of residues at average distance of 11.38 Å from H 50 produced similar kinetic data, as do mutations of residues at the average distance 14.42 Å. The latter cluster showed the highest increments of the association rates with respect to the wild-type association. Mutations that produce neutral fragments do not always decrease the rate, as expected. Indeed, mutation of the aspartate at the N-terminus of the light chain does not affect the rate, and neutralization of a glutamate residue in the heavy chain (H 46) produces an increase in the association rate.

Double mutations were performed on selected residues that were found particularly effective in increasing the reaction rate (see Table 3). Selected associations for double mutant fragments are listed in Table 4, in which antibody

TABLE 4 Relative rate constants for selected double mutant associations

Double Mutant (DM)	k_{DM}*	$k_{AB}{}^{\dagger} = k_A \cdot k_B$
E50Q+E35Q	0.33 ± 0.02	0.26 ± 0.03
Q89E+Q90E	1.23 ± 0.05	1.3 ± 0.07
N61D+Q90E	0.89 ± 0.04	1.26 ± 0.07
N61D+Q89E	1.2 ± 0.05	1.2 ± 0.06
N92D+N32D	1.61 ± 0.07	1.61 ± 0.08
N102D+N32D	1.30 ± 0.07	1.46 ± 0.08
N102D+N92D	1.33 ± 0.06	1.48 ± 0.08

Ionic Strength = 150 mM. Overall charge of the antibody fragments = −3e.

*k_{DM} is the simulated relative rate for the double mutant fragments. Relative rates are computed as specified in Table 1.

†k_{AB} is assumed to be a measure of the correlation between the two sites involved in the mutation. Thus, if k_{AB} is equal to the product of the individual rates of A and B, then sites A and B are independent.

fragments have an overall charge equal to −3e. The last column of Table 4 contains a prediction of double mutant relatives rates, according to an empirical rule based on single mutation relative rates (Sines et al., 1992). When the product of relative rates for two single mutations, which are independently operated at sites A and B, is equal to the simulated value of the corresponding double mutant association, sites A and B are supposed to be not correlated. This was the case for two pairs of residues: H 61–L 89 and L 92–H 32. In other cases, predicted rates are greater than the simulated ones, with the only exception of the key pair H 35–H 50.

Some of the selected mutant associations were also studied using the C2 criterion, with a view to exploring the importance of structural features versus electrostatic effects (data not shown in the Tables). In particular, we focused on two mutant associations involving Asn L 32 and Asn L 92, because residue L 92 is a contact residue (Braden et al., 1994) at the interface between Fab D44.1 and HEL. These mutations of type asn→asp produced an increase in the reaction rates (the strongest ones), and their double mutant is one of the two in our set that follows the previously mentioned product rule (see Table 4). The two asparagines, L 32 and L 92, may be considered independent with respect to the electrostatic steering. Their locations (protruding, at the interface outside the binding site) may explain why the reaction rate was increased strongly by addition of the negative charges. It is known that L 92 makes several contacts with residues on HEL: they include an asparagine, a threonine, an aspartate, and two glycines (Gibas et al., 1997). Moreover, in spite of the fact that L 92 and L 32 are very close to each other, they may not interact because of their location on the surface of the fragment.

DISCUSSION

Trends in ionic strength dependence of the reaction rates are comparable to the expected one, based on Debye–Huckel models with complex geometry. Indeed, mutant fragments that are neutral or positively charged have relative on-rates that are bigger at higher ionic strengths. We note here that there is a net positive charge on HEL. The (absolute) rate constant of the wild type association, in which the antibody fragment is negatively charged, decreases as the ionic strength increases, whereas the association rate of positively charged mutant fragment (key double mutant) increases with the ionic strength. Neutral antibody fragments, such as the key single mutants, show no dependence on the ionic strength.

We observe that mutation of H 50, E50Q, results in a larger reduction of the reaction rate than the mutation of the H 35, E35Q. Residue H 35 is farther from the mouth of the binding site than residue H 50. Glutamate H 50 is able to form two salt bridges with both the arginine residues of the lysozyme epitope, whereas glutamate H 35 is involved in one salt link only. This fact, along with kinetics results, seems to suggest that H 50 has a major role in the steering. In the case of DMU, comparison between simulated reaction rate (reaction criterion C2) and the product rule prediction suggests that these two key glutamates are independent as well (see Table 4).

The same qualitative trends are observed in the case of HyHEL-5 association (Kozack et al., 1995). However, ionic strength dependence and electrostatic steering of the D44.1-HEL association seem to be weaker than those for HyHEL-5-HEL. MAbs HyHEL-5 and D44.1 share similar on-rate constants, despite their different affinities for HEL. Unlike in the case of HyHEL-5, where a systematic dependence of the reaction rate on charged residues distance from the key glutamates H 35 and H 50 was observed, D44.1 does not display a similar trend. As in the work reported on HyHEL-5 (Kozack and Subramaniam, 1993), electrostatic steering was monitored in D44.1-HEL association. We observed the evolution of an ensemble of trajectories from their starting point on the b surface to the reaction sphere, centered in the C_δ atom of the key residue H 50. As expected, at large distance, the ensemble is homogeneous, whereas, in the vicinity of the antibody, where the electrostatic field is strongly asymmetric, the antigen is captured by the antibody's binding site. In addition to this brightest peak, a second spot of higher antigen density was observed on the trajectory histogram (Fig. 3). Such a "decoy site" was also reported in the case of HyHEL-5 (Kozack and Subramaniam, 1993). In the D44.1-HEL, it corresponds to a location that would not be exposed to the solvent in the Fab fragment or in their parent IgG.

The two different reaction criteria used to characterize the association produce comparable relative reaction rates. This can be seen in Fig. 5 for E35Q, which displays the ionic strength dependence of the relative reaction rate for key residue mutants. When the residue is responsible for strong electrostatic steering as in the case of H 50, the mutation results in impacting the choice of reaction criteria. In this

case use of C1 and C2 yield distinct relative rates (Fig. 5). In double mutant complexes that obey the independent residue rule (Table 4), both C1 and C2 criteria lead to relative rates that satisfy the product rule. For instance, in the double mutation involving L 32 and L 92 mutations, the relative rates obtained from simulation and from the product rule are comparable (1.61 ± 0.07 and 1.61 ± 0.08, respectively) for the C1 criterion and (1.80 ± 0.08 and 1.77 ± 0.15, respectively) for the C2 criterion. This is also true for the double mutant involving mutations of H 35 and H 50 for both C1 (Table 4) and C2 (simulation value 0.25 ± 0.02 and product rule 0.25 ± 0.03).

Orientation effects should have an important role in the association, as shown by results obtained with the reactive patch, and from modeling with a dumbbell. Based on experimental data on antibody–antigen association, the order of magnitude for on-rates in antibody–antigen association is expected to be of the order of 10^{6-1}. The spherical patch model reproduced this order of magnitude. In modeling with a dumbbell, our computed on-rates match the experimental results obtained for the HyHEL-5-HEL association (Xavier and Willson, 1998). Absolute rates computed with reactive patch and dumbbell model differ by about one order of magnitude. This could be expected from the fact that reaction probability computed with dumbbell provides an upper estimate of the actual reaction probability, because dumbbell provides looser orientation constraints than the spherical patch does. Reaction rates for HyHEL-5 have been measured using stopped-flow methods (Xavier and Willson, 1998). At ionic strength 150 mM, the association rate is reported to be $2.4 \pm 0.2 \times 10^{7-1}$, while the corresponding computed value (Kozack et al.1995) is $1.7 \times 10^{6-1}$. The experimental value should be taken as an upper estimate of the actual rate (R. C. Willson, personal communication). It is also important to point out that reaction rates are essentially affected by the choice of the diffusion coefficient. We actually used two different diffusion coefficients in computing reaction rates within the two models' frames, the spherical patch model and the dumbbell. In spite of the fact that antigen sphere model is essentially structureless, predictions of relative rates are quite reliable, because they do not depend on a scaling factor. It was already pointed out (Kozack and Subramaniam, 1993) that the sphere model has the major advantage of allowing the testing of a large number of mutant associations in a reasonable computational time. In our present work, obtaining on-rate constant at ionic strength 150 mM required a computational time 20 times longer, with the antigen modeled as a dumbbell.

Studies on pKa of the glutamates and aspartates in the D44.1 Fv fragment (Gibas et al., 1997) showed that these residues, more than other titrating residues, change their protonation states upon association giving way to a complex pattern of fractional charges. This was a rationale for studying their mutations. Mutations were done in such a way that they did not appreciably affect the structure. Our mutations should be called "steering" mutations, because we have no way to assess how that specific substitution affects the three-dimensional structure of the protein.

To understand what structural feature makes a mutation more or less effective (in terms of deviation from the rate of the wild type association), we evaluated kinetic data in terms of mutant residue distances from the C_δ atom of both H 50 and H 35. In analyzing negative mutations (−2e) with respect to increasing distances from H 35, we observed an increase in the rates with the only exception of mutant N61D. Looking at the H 50 distances, we found more exceptions. Neutral mutations also showed a similar trend. We observed that association rates increase with distance from H 35, with the exception of E46Q. On the whole, no strong correlation between distance from key residues and reaction rates are observed. Presence of voids and water molecules at the interface of the complex will have a role in the association, but they were not explicitly taken into account in our study. The analysis of the geometry of the residue clusters showed that residues within the pairs L 90–L 89, H 102–L 32, and H 102–L 92 interact strongly, because there is no screening between them. Moreover, they are buried in a low dielectric environment of the protein. The residues in the pair L 92–L 32 do not interact strongly, instead, because they are at the surface of the antibody and have a large solvent accessibility. They are also oriented in a manner such that the addition of negative charges can steer the antigen toward the mouth of the combining site.

Interestingly, simultaneous mutations of the residues pair L 32 and L 92, and of the two key residues H 35 and H 50, reproduced the product of the corresponding single mutant rates (Table 4). Residue L 92 contacts a number of residues on HEL, which may explain the double mutation kinetic results. Residues H 61 and L 89 are far away from each other (distance of L 89 atom C_δ from H 61 atom C_γ is 13.41 Å) and screened by several side chains, including the key residues, an arginine and a tryptophan. Their interaction is weaker than in the other cases, and this explains their kinetic independence.

CONCLUSION

Brownian Dynamics serves as a valuable computational tool for quantitatively assessing important biochemical process, such as protein–protein association. Correct order of magnitude of on-rate constants for antibody fragment–protein antigen interactions can be reproduced, and biochemical information can be extracted from this type of computer simulation. From the comparison of the two associations, D44.1-HEL and HyHEL-5-HEL, we can draw a specific conclusion. The affinity of the HyHEL-5-HEL is 4×10^{10} M^{-1} (Hibbits et al., 1994), whereas affinity of D44.1-HEL is 1.4×10^7 M^{-1} (Tello et al., 1993). From our study, their on-rate constants are apparently similar, whereas the off-rate of HyHEL-5-HEL was reported to be $\sim 3.2 \times 10^{-5}$ s^{-1}

(Xavier and Willson, 1998). Assuming that the on-rates are the same for mAbs HyHEL-5 and D44.1, the off-rate of mAb D44.1 should be 9×10^{-2} s^{-1}. Thus, the origins of difference in the affinity of binding of the two antibodies to HEL lie in the off-rates of the complex.

The implication of this result can be especially interesting in immunology. The canonical view has been that the leitmotif for maturation is affinity to the antigen, i.e., after a prolonged time period after exposure to the antigen, the antibodies found in the serum have reached a plateau of affinity for the antigen, and the maturation process is complete (Eisen, 1966). This paradigm was based on antibodies isolated from mice at different time periods after exposure to haptens such as 2,4-dinitrophenyl groups (Eisen and Siskind, 1964). Future exposure to the antigen, after the antibodies have reduced to the background level, shows that the memory B-cells are those encoding high-affinity antibodies.

Recent experiments on the antibody maturation process appear to contradict the canonical view, in that the antibodies obtained early in the response period not only have reached very high affinities, but also the maturation process appears to be driven by the kinetics of encounter as opposed to affinity. It is possible that the on-rates of the DNP system are already so high in the primary antibodies that a further optimization is unnecessary and hence not selected. In hybridomas generated at well-defined intervals after immunization of mice with lysozyme (Newman et al., 1992), and with vesicular stomatitis virus (Roost et al., 1995), it was found that very high affinity antibodies are generated very early in the response (within 6 days) and, further, the affinity does not increase in response to repeated boosting for a longer period. More importantly, Roost et al. (1995) find that there is a stronger correlation of virus neutralization with on-rates than with affinity, implying that the maturation process is driven by the kinetics of antibody–antigen encounter (Foote and Milstein, 1991). More recently, Batista and Neuberger (1998) have studied the anti-lysozyme antibody system and probed the role of kinetics in maturation. Given the degree of accuracy achieved in modeling three dimensional structures of antibody fragments, simulation methods such as the one described here will be useful in studying the rates of association for generations of monoclonal antibodies and help shed light on the maturation phenomenon.

APPENDIX

The inequality in Eq. 10 is straightforward if we note that the rate constant of Eq. 4 can be written in an alternative way, dividing both the numerator and denominator by β:

$$k(\beta) = \frac{1}{A/\beta + B}, \quad A \equiv I(b, q), \quad B \equiv I(q, \infty), \tag{A1}$$

where A and B are two constants, and $I(x_1, x_2)$ is the integral

$$I(x_1, x_2) = \int_{x_1}^{x_2} \frac{\exp[U(r)/K_B T]}{r^2}\, dr, \tag{A2}$$

in which $U(r)$ is the centrosymmetric energy function, and $K_B T$ is the thermal energy. The integral $I(x_1, x_2)$ is linked to the analytical rate $k_D(x)$ by definition

$$k_D(x) = 4\pi D \frac{1}{I(x, \infty)}. \tag{A3}$$

To show the validity of Eq.12, we just note that Eq. A1 can be also written in as

$$k(\beta) = \frac{C}{(1 - \Omega)/\beta + \Omega}, \tag{A4}$$

where Ω is the ratio of $k_D(b)$ and $k_D(q)$, and C is the value of $k_D(b)$ alone. If $(1 - \Omega)/\beta \gg \Omega$, Eq. A4 becomes

$$k(\beta) \approx \beta * \frac{C}{1 - \Omega} \propto \beta. \tag{A5}$$

In our simulation, Ω is 0.160001, so $1 - \Omega \sim 1$, and the highest value of β is of the order of 1/100 (WT association). The inequality above is satisfied, and, in first approximation, the reaction rate will be directly proportional to the scaling factor p.

We thank Gang Zou and David Bock for trajectories' analysis and visualization, and Cynthia Gibas for help with UHBD software. This work was partially supported by an Istituto Pasteur–Fondazione Cenci Bolognetti Fellowship to G.A. and by National Science Foundation grant DBI 96–04223, and National Institutes of Health grant GM 46535 to S.S. We also wish to acknowledge a Metacenter Supercomputing Allocation at the National Center for Supercomputing Applications.

REFERENCES

Batista, F. D., and M. S. Neuberger. 1998. Affinity dependence of the B cell response to antigen: a threshold, a ceiling, and the importance of the off-rate. *Immunology.* 8:751–759.

Berg, O. G., and P. H. von Hippel. 1985. Diffusion-controlled macromolecular interactions. *Ann. Rev. Biophys. Biophys. Chem.* 14:131–160.

Bhat, T. N., G. A. Bentley, T. O. Fischmann, G. Boulot, and R. J. Poljack.1990. Small rearrangements in structures of Fv and Fab fragments of antibody D1.3 on antigen binding. *Nature.* 317:483–485.

Braden, B. C., H. Souchon, J. L. Eisele, G. A. Bentley, T. N. Bhat, J. Navaza, and R. J. Poljak. 1994. Three-dimensional structures of the free and antigen-complexed Fab from monoclonal anti-lysozyme antibody D44.1. *J. Mol. Biol.* 243:767–781.

Braden, B. C., and R. J. Poljack. 1995. Structural features of the reactions between antibodies and protein antigens. *FASEB.* 9:9–16.

Chandrasekhar, S. 1946. Stochastic problem in physics and astronomy. *Rev. Mod. Phys.* 15:1–82.

Davies, D. R., and G. H. Cohen. 1996. Interactions of protein antigens with antibodies. *PNAS.* 93:7–12.

Davies, D. R., and J. A. McCammon . 1990. Electrostatics in biomolecular structure and dynamics. *Chem. Rev.* 90:509–521.

Eisen, H. N. 1966. The immune response to a simple antigenic determinant. *Harvey Lect.* 60:1–34.

Eisen, H. N., and G. W. Siskind. 1964. Variations in affinities of antibodies during the immune response. *Biochem.* 3:996–1008.

Ermak, D. L., and, J. A. McCammon.1978. Brownian dynamics with hydrodynamic interactions. *J. Chem. Phys*. 69:1352–1360.

Foote, J., and C. Milstein. 1991. Kinetic maturation of an immune response. *Nature.* 352:530–532.

Foote, J., and H. N. Eisen . 1995. Kinetic and affinity limits on antibodies produced during immune response. *PNAS.* 92:1254–1256.

Gabdoulline, R. R., and R. C. Wade. 1997. Simulation of the diffusional association of Barnase and Barstar. *Biophys. J.* 72:1917–1929.

Gabdoulline, R. R., and R. C. Wade. 1999. On the protein–protein diffusional encounter complex. *J. Mol. Recognit.* 12:226–234.

Gibas, C. J., S. Subramaniam, J. A. McCammon, B. C. Braden, and R. J. Poljak. 1997. pH dependence of antibody/lysozyme complexation. *Biochemistry* 36:15599–15614.

GRASP: Nicholls, A., K. Sharp, and B. Honig. 1991. Protein folding and association: insight from the interfacial and thermodynamic properties of hydrocarbons. *Proteins Struct. Funct. Genet.* 11:281–296.

Hibbits, K. A., D. S. Gill, and R. C. Willson. 1994. Isothermal titration calorimetric study of the association of hen egg lysozyme and the anti-lysozyme antibody HyHEL-5. *Biochemistry.* 33:3584–3590.

Hynes, J. T.1985. The theory of reactions in solution. *In* The Theory of Chemical Reaction Dynamics. Vol. IV. M. Baer, editor. CRC Press, Boca Raton, FL.

Hubbard, S. J., and J. M. Thornton. 1993. NACCESS. Computer program, Department of Biochemistry and Molecular Biology, University College, London, U.K.

Koehler, G., and C. Milstein. 1975. Continuous cultures of fused cells secreting antibody of predefined specificity. *Nature.* 256:495–497.

Kozack, R. E., and S. Subramaniam. 1993. Brownian dynamics simulations of molecular recognition in an antibody–antigen system. *Protein Sci.* 2:915–926.

Kozack, R., M. J. d'Mello, and S. Subramaniam.1995. Computer modeling of electrostatic steering and orientational effects in antibody–antigen association. *Biophys. J.* 68:807–814.

Madura, J. D., J. M. Briggs, R. C. Wade, M. E. Davies, B. A. Luty, A. Ilin, J. Antosiewicz, M. K. Gilson, B. Bagheri, L. R. Scott, and J. A. McCammon. 1995. Electrostatics and diffusion of molecules in solution: simulations with the University of Houston Brownian Dynamics program. *Comp. Phys. Comm.* 91:57–95.

Newman, M. A., C. R. Mainhart, C. P. Mallet, T. B. Lavoie, and S. J. Smith-Gill.1992. Patterns of antibody specificity during the BALB/c immune response to hen egg lysozyme. *J. Immunol.* 149:3260–3272.

Northrup, S. H., and H. P. Erickson. 1992. Kinetics of protein–protein association explained by Brownian dynamics computer simulation. *PNAS.* 89:3338–3342.

Northrup, S. H., S. A. Allison, and J. A. McCammon. 1984. Brownian dynamics simulation of diffusion-influenced bimolecular reactions. *J. Chem. Phys.* 80:1517–1524.

QUANTA. Molecular modeling software package.1996. Molecular simulations, Inc., San Diego, CA.

Raman, C. S., R. Jemmerson, B. T. Nall, and M. J. Allen. 1992. Diffusion-limited rates for monoclonal antibody binding to cytochrome *c*. *Biochemistry.* 31:10370–10379.

Roost, H., M. F. Bachmann, A. Haag, U. Kaline, V. Pliska, H. Hengartner, and R. M. Zinkernagel. 1995. Early high-affinity neutralizing anti-viral IgG responses without further overall improvements of affinity. *PNAS.* 92:1257–1261.

Schwartz, F. P., D. Tello, F. A. Goldbaum, R. A. Mariuzza, and R. J. Poljak. 1995. Thermodynamics of antigen–antibody binding using specific anti-lysozyme antibodies. *Eur. J. Biochem*. 228:388–394.

Smoluchowski, M. V. 1917. Versuch einer mathematischen Theorie der Koagulationskinetik kolloider Loeschungen. *Z. Phys. Chem.* 92: 129–168.

Sines, J. J., J. A. McCammon, and S. A. Allison. 1992. Kinetics effects of multiple charge modifications in enzyme–substrate reactions: Brownian dynamics simulations of Cu, Zn superoxide dismutase. *J. Comp. Chem.* 13:66–69.

Tello, D., F. A. Goldbaum, R. A. Mariuzza, X. Ysern, F. P. Schwartz, and R. J. Poljack. 1993. Three-dimensional structure and thermodynamics of antigen binding by anti-lysozyme antibodies. *Biochem. Soc. Trans*. 21:943–946.

Xavier, K. A., and R. C. Willson. 1998. Association and dissociation kinetics of anti-hen egg lysozyme monoclonal antibodies HyHEL-5 and HyHEL-10. *Biophys. J.* 74:2036–2045.

Van Kampen, N. G. 1992. Stochastic Processes in Physics and Chemistry. 2nd edition. North Holland, Amsterdam.

Warwicker, J., and H. C. Watson. 1982. Calculation of the electric potential in the active site cleft due to alpha-helix dipoles. *J. Mol. Biol.* 157: 671–679.

Wade, R. C. 1996. Brownian dynamics simulations of enzyme–substrate encounter. *Biochem. Soc. Trans.* 24:254–259.

Winter, G., and C. Milstein. 1991. Man-made antibodies. *Nature.* 349: 293–299.

Zhou, H. 1993. Brownian dynamics study of the influences of electrostatic interaction and diffusion on protein–protein association kinetics. *Biophys. J.* 64:1711–1726.